

Reconstructing baryon oscillations

Yookyung Noh,^{1,*} Martin White,^{2,†} and Nikhil Padmanabhan^{3,‡}

¹*Department of Astronomy, 601 Campbell Hall, University of California Berkeley, CA 94720*

²*Departments of Physics and Astronomy, 601 Campbell Hall, University of California Berkeley, CA 94720*

³*Dept. Physics, Yale University, New Haven, CT 06511*

(Dated: November 1, 2018)

The baryon acoustic oscillation (BAO) method for constraining the expansion history is adversely affected by non-linear structure formation, which washes out the correlation function peak created at decoupling. To increase the constraining power of low z BAO experiments, it has been proposed that one use the observed distribution of galaxies to “reconstruct” the acoustic peak. Recently Padmanabhan, White & Cohn provided an analytic formalism for understanding how reconstruction works within the context of Lagrangian perturbation theory. We extend that formalism to include the case of biased tracers of the mass and, because the quantitative validity of LPT is questionable, we investigate reconstruction in N-body simulations. We find that LPT does a good job of explaining the trends seen in simulations for both the mass and for biased tracers and comment upon the implications this has for reconstruction.

PACS numbers:

I. INTRODUCTION

It has been known for many years that the coupling of photons and baryons in the early universe results in significant features in the matter power spectrum [1, 2, 3]. Prior to recombination, photons and baryons are tightly coupled and are well approximated by a fluid. Perturbations during this epoch do not grow, but instead excite sound waves which get frozen at recombination and manifest themselves as an almost harmonic series of peaks in the power spectrum, $P(k)$, or equivalently a narrow feature in the correlation function, $\xi(r)$ (see [4, 5] for a detailed description of the physics in modern cosmologies and [6] for a comparison of Fourier and configuration space pictures). These so-called “baryon acoustic oscillations” (BAO) can be used as a standard ruler to measure the expansion rate of the Universe, making the method an integral part of current and next-generation dark energy experiments.

While the early Universe physics is linear and well understood, the low redshift observations are complicated by the non-linear evolution of matter, galaxy bias and redshift space distortions. The non-linear evolution leads to a coupling of k -modes and damping of the oscillations on small scales [4] and a small shift in their positions [6, 7, 8, 9, 10]. The damping of the linear power spectrum (or equivalently the smoothing of the correlation function) reduces the contrast of the feature and the precision with which the size of ruler may be measured.

In [6] it was pointed out that much of the modification to the power spectrum comes from bulk flows and super-cluster formation. Since these large-scale flows are reasonably well measured by the survey, their effects can, in principle, be corrected. In [11] a method was introduced for removing the non-linear degradation of the acoustic signature, sharpening the feature in configuration space or restoring/correcting the

higher k oscillations in Fourier space; this method has been tested on simulations by a number of groups [11, 12, 13]. However, this method is inherently non-linear and therefore difficult to understand analytically. A study of this problem for the matter density using Lagrangian perturbation theory [14] explained how the method “reconstructed” the BAO feature, but also pointed out that it did not reconstruct the linear density field. We extend these results here - (i) generalizing the analytic theory to biased tracers, including explicit expressions for the reconstructed power spectrum to second order in the linear power spectrum, and (ii) testing the validity of the analytic expressions with a suite of N-body simulations.

We compare the analytic theory to a set of 1024^3 particle simulations run in periodic, cubical boxes of side length $2 h^{-1}\text{Gpc}$ with a *TreePM* code [15]. The simulations were initialized at $z = 100$ using second order Lagrangian perturbation theory, and the phase space information for all of the particles was dumped at $z = 0, 0.3, 0.7$ and 1.0 . Multiple realizations, with different initial density fields, were run for each cosmology to reduce sampling effects (more details can be found in [10, 16]). In addition to the dark matter particle data, halo catalogs were produced for each output using the friends-of-friends method [17] with a linking length of 0.168 times the mean inter-particle spacing. We work with halos above $10^{13} h^{-1}M_{\odot}$, i.e. containing more than 20 particles.

We investigate one of the cosmologies considered in [10, 16]: ΛCDM , with $\Omega_M = 0.25$, $\Omega_B = 0.04$, $h = 0.72$, $n = 0.97$ and $\sigma_8 = 0.8$. This is close to the current “best fit” cosmology and will serve as a realistic model to explore. Within this cosmology the acoustic peak in the correlation function is at $\sim 110 h^{-1}\text{Mpc}$, with an intrinsic width set by the diffusion (Silk) damping scale of $\sim 10 h^{-1}\text{Mpc}$.

II. RECONSTRUCTION I: MATTER

We begin our investigation of reconstruction by considering the most conceptually simple case: reconstruction of the acoustic peak in the matter 2-point function. We start by re-

*Electronic address: ynoh@astro.berkeley.edu

†Electronic address: mwhite@berkeley.edu

‡Electronic address: nikhil.padmanabhan@yale.edu

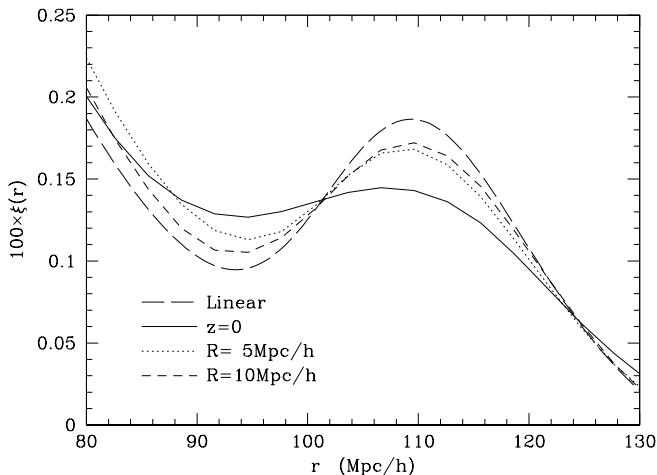


FIG. 1: The mass correlation function for our Λ CDM model at $z = 0$ before (solid) and after reconstruction using a smoothing of $R = 5 h^{-1}$ Mpc (dotted) and $R = 10 h^{-1}$ Mpc (short dashed). Non-linear evolution has partially erased the peak in the initial conditions (long-dashed) by $z = 0$, but it is somewhat restored by reconstruction.

viewing the reconstruction algorithm of [11] and its interpretation within Lagrangian perturbation theory [14], and then compare its predictions with simulations. The following section extends this analysis to biased tracers.

A. Algorithm

The algorithm devised by [11] is straightforward to apply to a simulation and consists of the following steps:

- Smooth the density field to filter out high k modes, which are difficult to model.
- Compute the negative Zel’dovich displacement, \mathbf{s} , from the smoothed density field: $\mathbf{s}(\mathbf{k}) = -i(\mathbf{k}/k^2)\delta(\mathbf{k})\mathcal{S}(k)$, where \mathcal{S} is the smoothing kernel (see below).
- Shift the original particles by \mathbf{s} and compute the “displaced” density field, δ_d .
- Shift an initially spatially uniform distribution of particles by \mathbf{s} to form the “shifted” density field, δ_s .
- The reconstructed density field is defined as $\delta_r \equiv \delta_d - \delta_s$ with power spectrum $P_r(k) \propto \langle |\delta_r^2| \rangle$.

Following [11] we use a Gaussian smoothing of scale R , specifically

$$\mathcal{S}(k) = e^{-(kR)^2/2} . \quad (1)$$

We take advantage of the periodicity of the simulations to perform all of these steps using fast Fourier transforms. The density fields are constructed from the particle positions using a CIC assignment [18].

Fig. 1 shows an example of reconstruction, for the Λ CDM model. By $z = 0$ non-linear evolution has partially washed out the peak in the matter correlation function (solid line). However applying reconstruction with $R = 5$ or $10 h^{-1}$ Mpc restores much of the original signal. Fig. 2 shows reconstruction at the level of the density fields, for a thin slice through a piece of one of our simulations centered on a halo of mass $4 \times 10^{14} h^{-1} M_\odot$. We see that reconstruction has ‘reversed’ the formation of collapsed structures, and yields a field that is visually similar to the initial density field. Note the final field has sharper, more pronounced peaks than either the initial or reconstructed density fields, though the reconstructed field still has more prominent peaks than the initial field.

B. Lagrangian perturbation theory

Reconstruction naturally lends itself to a description in terms of Lagrangian perturbation theory, which we briefly review here. The Lagrangian description of structure formation [19, 20, 21] relates the current (or Eulerian) position of a mass element, \mathbf{x} , to its initial (or Lagrangian) position, \mathbf{q} , through a displacement vector field $\Psi(\mathbf{q})$,

$$\mathbf{x} = \mathbf{q} + \Psi(\mathbf{q}) . \quad (2)$$

The displacements can be related to overdensities by [22]

$$\delta(\mathbf{k}) = \int d^3q e^{-i\mathbf{k}\cdot\mathbf{q}} \left(e^{-i\mathbf{k}\cdot\Psi(\mathbf{q})} - 1 \right) . \quad (3)$$

Analogous to Eulerian perturbation theory, LPT expands the displacement in powers of the linear density field, δ_L ,

$$\Psi = \Psi^{(1)} + \Psi^{(2)} + \dots , \quad (4)$$

with $\Psi^{(n)}$ being n^{th} order in δ_L . First order in LPT is equivalent to the well-known Zel’dovich approximation.

In the simulations the rms ($1D$) displacement goes from $6.1 h^{-1}$ Mpc at $z = 0$ to $3.9 h^{-1}$ Mpc at $z = 1$, in excellent agreement with the expectations of the Zel’dovich approximation. In fact the Zel’dovich rms displacements match those measured in the simulations at the percent level, better than we would expect given the size of the second order corrections.

Using Eq. (3) the power spectrum is

$$P(k) = \int d^3q e^{-i\mathbf{k}\cdot\mathbf{q}} \left(\langle e^{-i\mathbf{k}\cdot\Delta\Psi} \rangle - 1 \right) , \quad (5)$$

where $\mathbf{q} = \mathbf{q}_1 - \mathbf{q}_2$, and $\Delta\Psi = \Psi(\mathbf{q}_1) - \Psi(\mathbf{q}_2)$. Expanding the exponential in powers of Ψ and using Eq. (A1) reproduces the results of “standard” perturbation theory. However, following [9], if we use the cumulant expansion theorem to expand the exponential and expand the resulting powers of $\mathbf{k} \cdot \Delta\Psi$ using the binomial theorem we have two types of terms: those where the Ψ are all evaluated at the same point (which we can take to be the origin) and the rest. Leaving the first set of terms exponentiated while expanding the second set of terms in powers of Ψ , we find

$$P(k) = e^{-k^2\Sigma^2/2} \{P_L(k) + \dots\} \quad (6)$$

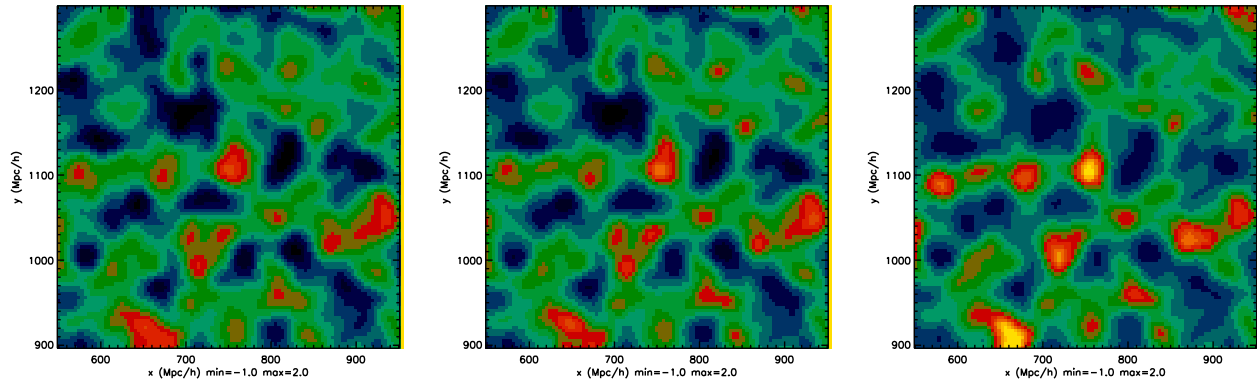


FIG. 2: A thin slice through a simulation showing the initial (left), reconstructed (middle) and final (right) density fields all smoothed with a Gaussian of $10 h^{-1} \text{Mpc}$. Each slice is centered on the (final) position of a halo of mass $4 \times 10^{14} h^{-1} M_{\odot}$. Note the final field has sharper, more pronounced peaks than either the initial or reconstructed density fields, though the reconstructed field still has more prominent peaks than the initial field.

R	$z = 0$				$z = 1$			
	Shifted Sim	Shifted 1LPT	Displaced Sim	Displaced 1LPT	Shifted Sim	Shifted 1LPT	Displaced Sim	Displaced 1LPT
5	5.82	5.39	3.35	1.95	3.76	3.41	2.16	1.23
10	4.92	4.80	3.40	2.80	3.20	3.04	2.19	1.77
15	4.39	4.34	3.72	3.36	2.85	2.75	2.38	2.13
20	3.99	3.97	4.00	3.77	2.59	2.52	2.56	2.38
25	3.67	3.67	4.24	4.07	2.39	2.32	2.71	2.58
30	3.40	3.41	4.45	4.32	2.21	2.16	2.84	2.73

TABLE I: The rms displacements of the “shifted” and “displaced” particles at $z = 0$ and $z = 1$ as a function of the smoothing scale R . First order LPT correctly predicts the observed displacements (at the 10% level), with the agreement improving as the smoothing scale increases.

where $P_L(k)$ is the linear theory power spectrum, Σ is proportional to the rms Zel’dovich displacement (i.e. final minus initial particle positions to linear order)

$$\Sigma^2 = \frac{1}{3\pi^2} \int dq P_L(p) \quad (7)$$

and explicit expressions for the higher order terms may be found in [9] and Appendix A. The exponential prefactor describes the broadening of the acoustic peak seen in Fig. 1, some of the additional terms lead to a slight change in the peak position [8, 10, 14]. The rms displacement of an individual particle is $\Sigma/\sqrt{2}$.

The effects of the exponential prefactor are most easily seen by considering the correlation function. Furthermore, Lagrangian perturbation theory, like several other perturbation theory schemes, performs better at predicting the large-scale correlation function than the power spectrum, since it fails to accurately predict broad-band power which contributes at small r [9, 10]. For these reasons, we shall present most of our comparisons between theory and simulation in configuration space, i.e. we shall present

$$\xi(r) = \int \frac{d^3 k}{(2\pi)^3} P(k) j_0(kr) = \int \frac{dk}{k} \Delta^2(k) j_0(kr) \quad (8)$$

with $j_0(x) = \sin(x)/x$ the spherical Bessel function of order zero. This comparison also has the advantage of more clearly emphasizing the acoustic feature, which can be easily seen as a single peak in $\xi(r)$ at $r \sim 110 h^{-1} \text{Mpc}$. For presentation purposes we have smoothed all of the correlation functions by $3 h^{-1} \text{Mpc}$ before plotting them – this reduces high frequency noise in the N-body simulations but has a minimal impact on the shape of the curves since this smoothing adds in quadrature to the $\sim 10 h^{-1} \text{Mpc}$ intrinsic width of the features. Observationally one could achieve similar effects by using broad but overlapping r bins.

A second interesting statistic is the cross-spectrum between the linearly evolved initial field, δ_L and the fully evolved final field, δ_f ,

$$G_f(k) \equiv \frac{\langle \delta_L(k) \delta_f^*(k) \rangle}{P_L} \quad (9)$$

sometimes referred to as the propagator [8]. The relevant physics in this case is more cleanly visualized in Fourier space, since it shows the decorrelation between the initial field and the processed field which becomes a convolution in configuration space. Fits to numerical simulations [6] and a variety of analytic arguments [6, 7, 8, 9, 10, 14, 23], including Lagrangian perturbation theory, suggest that

$$G_f(k) \simeq e^{-(k\Sigma)^2/4} + \dots \quad (10)$$

i.e. that the damping is half as strong as in the power spectrum (see Appendix A for expressions beyond leading order).

It is straightforward to repeat these steps for the reconstructed field [14]. We assume that the density field is smoothed on a large enough scale that \mathbf{s} can be approximated as $\mathbf{s} = -i(\mathbf{k}/k^2)\delta_L(\mathbf{k})\mathcal{S}(k)$. We can then compare the three contributions to the power spectrum (P_{ss} , P_{dd} and P_{sd}) to get

the reconstructed power spectrum [14]

$$P_r(k) = \left\{ e^{-k^2 \Sigma_{ss}^2/2} \mathcal{S}^2(k) + 2e^{-k^2 \Sigma_{sd}^2/2} \mathcal{S}(k) \bar{\mathcal{S}}(k) + e^{-k^2 \Sigma_{dd}^2/2} \bar{\mathcal{S}}^2(k) \right\} P_L(k) + \dots \quad (11)$$

where $\bar{\mathcal{S}} \equiv 1 - \mathcal{S}$, and as before, the higher order terms are Appendix A. There are now three smoothing terms, (Σ_{ss} , Σ_{dd} and Σ_{sd}) defined by

$$\Sigma_{ss}^2 \equiv \frac{1}{3\pi^2} \int dq P_L(p) \mathcal{S}^2(p), \quad (12)$$

$$\Sigma_{dd}^2 \equiv \frac{1}{3\pi^2} \int dq P_L(p) \bar{\mathcal{S}}^2(p), \quad (13)$$

and $\Sigma_{sd}^2 = (\Sigma_{ss}^2 + \Sigma_{dd}^2)/2$ (see Table I). As pointed out in Ref. [14], all of these smoothing scales are smaller than the nonlinear smoothing Σ , explaining why the acoustic feature is sharpened after reconstruction. A related calculation (see Appendix A) yields the propagators

$$G_f = e^{-k^2 \Sigma^2/4} + \dots \quad (14)$$

$$G_d = e^{-k^2 \Sigma_{dd}^2/4} \bar{\mathcal{S}} + \dots \quad (15)$$

$$G_s = e^{-k^2 \Sigma_{ss}^2/4} [-\mathcal{S}] + \dots \quad (16)$$

$$G_r \equiv G_d - G_s, \quad (17)$$

with the higher order terms in the Appendix.

C. Comparison with simulations

To begin we compare the predictions of perturbation theory for the propagator to calculations of the same quantity in N-body simulations. This isolates the damping behavior from the mode-coupling [10]. Fig. 3 shows the different contributions to the reconstructed propagator. The theoretical predictions for G_f are in reasonably good agreement with the results, with the theory showing slightly weaker damping than the simulations. (Small changes to the theoretically predicted Σ can bring the results into much better agreement, but we will not make such *ad hoc* changes here.) The agreement is somewhat worse for some pieces of the reconstructed propagator. In particular the simulations show that the reconstructed field retains better memory of its initial conditions ($G_r \approx 1$) at intermediate scales than LPT predicts, with perturbation theory giving too much power at high k . The over-prediction at high k is not of particular concern, since at these scales the dimensionless power exceeds unity and we would expect perturbation theory to be breaking down. Out to $k \simeq 0.2 h \text{ Mpc}^{-1}$, where $\Delta^2 \sim 1$, perturbation theory agrees with the simulations at the better than 10% level! We emphasize that this level of agreement comes from the inclusion of the 2nd order contributions, with the dominant correction coming from the R_1 term (see Appendix A).

Fig. 4 shows the corresponding figure for the correlation functions, broken down into the same components. Note the

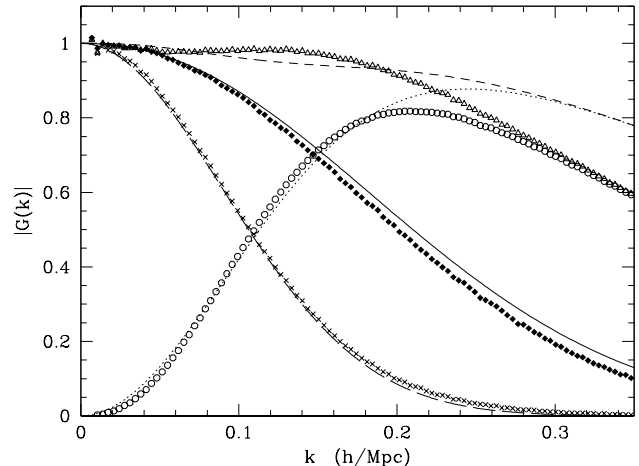


FIG. 3: The cross-correlation between the linearly evolved initial field and the fully evolved final field, displaced field, shifted field and the reconstructed field for Λ CDM at $z = 0$ (see text). The points show the results of N-body simulations while the lines show the predictions from Lagrangian perturbation theory [14]. The solid line and diamonds represent $G_f(k)$, the dotted line and circles represent $G_d(k)$, long-dashed line and crosses represent $G_s(k)$ and short-dashed line and triangles represent $G_r(k)$. We have used a smoothing of $R = 10 h^{-1} \text{ Mpc}$.

excellent agreement for the displaced and shifted fields, but less good agreement for the final and reconstructed fields. In this figure the level of agreement between ξ_f and the theory is worse than the comparable figure in [24]. This is most likely due to the lower redshift and different cosmology we have chosen (see also [16]). The sense of the disagreement in both ξ_f and ξ_r is the same however, indicating that the Lagrangian perturbation theory of reconstruction is working better in a differential than absolute sense. As above, a small change in the relevant Σ could slightly improve the agreement with simulations, which may argue for leaving Σ as a free parameter when fitting to data. We will not pursue such modifications further here.

III. RECONSTRUCTION II: BIASED TRACERS

Unfortunately we don't directly measure the mass field in galaxy surveys, we measure the distribution of biased tracers. Here we investigate how the biasing of the tracers affects reconstruction. Rather than attempt a 'realistic' galaxy model, we shall concentrate on mass limited samples of halos when comparing LPT to the simulations. None of the essential aspects are lost with this simplification.

Reconstruction assumes that we can estimate the appropriate shifts from our smoothed, biased, density field. This requires that the smoothed halo field be a multiple of the smoothed mass field with known constant of proportionality (the bias). In the simulations we estimate the bias from the $k \approx 0$ limit of the propagator, in observations it would need

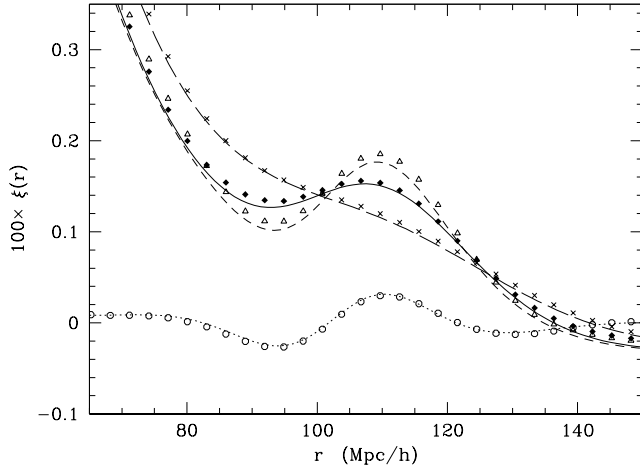


FIG. 4: The correlation functions of the fully evolved final, displaced, shifted, and reconstructed mass fields for Λ CDM at $z = 0$ (see text). As in Fig. 3 the points show the results of N-body simulations while the lines show the predictions from Lagrangian perturbation theory [14]. Solid line and diamonds represent ξ_f , dotted line and circles represent ξ_d , long-dashed line and crosses represent ξ_s , and short-dashed line and triangles represent ξ_r . We have used a smoothing of $R = 10 h^{-1} \text{Mpc}$.

to be determined in a different manner.

If we keep the denominator in Eq. (9) as the linear mass power spectrum, the lowest order modification to the propagator is to multiply by the linear bias of the tracer. The gross shape of $G(k)$ is unaltered, since the exponential damping is unchanged, being generated by the velocities which are sourced by the mass field not the halo field. At higher order, the cross terms between the linear and n th order terms are modified and introduce an additional dependence on the bias [24], as shown in Fig. 5. LPT predicts that the halo propagator falls slightly more slowly to high k than the mass propagator and the decline is slower the higher the mass threshold. This means that the halo propagator departs more from the Gaussian form than the mass propagator. It is possible that this is related to the special locations in the velocity field that rare, highly biased peaks occupy (e.g. [25, 26]). However, the difference is small, as shown explicitly in Fig. 5.

Fig. 6 shows the different propagators for halos more massive than $10^{13} h^{-1} M_\odot$ in the simulations and in theory. As was the case for the mass, the asymptote at high k is not well determined by the theory but the agreement at low k is quite good. G_s is the same as for the mass, and again the agreement between simulation and theory is good. The match between simulations and theory for G_f is quite good. Perturbation theory is correctly predicting the low k asymptote of G_d , which is no longer zero but $b - 1$, though it doesn't match the shape as well as for the mass. Once more the N-body simulations predict a G_r which increases slightly at intermediate k and is above the theory for $k \simeq 0.1 - 0.2 h \text{Mpc}^{-1}$.

To lowest order (see Appendix A for 2nd order contribu-

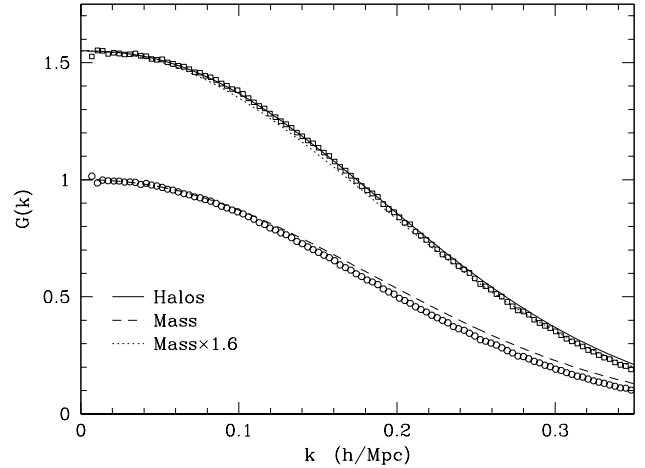


FIG. 5: The cross-correlation between the linearly evolved initial field and the fully evolved final field for the mass (dashed line and circles) and for halos above $10^{13} h^{-1} M_\odot$ (solid line and squares) in Λ CDM at $z = 0$. The dotted line shows the mass propagator multiplied by $b \simeq 1.6$.

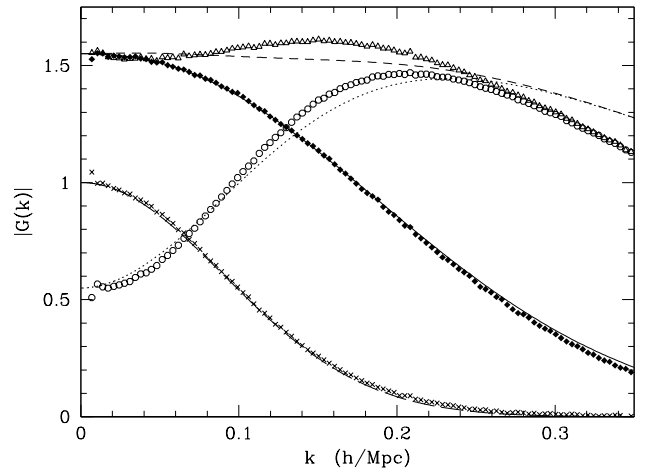


FIG. 6: The cross-correlation between the linearly evolved initial field and the evolved, displaced, shifted and reconstructed fields for halos above $10^{13} h^{-1} M_\odot$. Diamonds and the solid line show the final field, crosses and the long-dashed line the shifted field, circles and the dotted line the displaced field and the triangles and short-dashed line the reconstructed field.

tions) the reconstructed field has

$$P_r^{(0)}(k) = P_L(k) \left\{ e^{-k^2 \Sigma_{ss}^2/2} \mathcal{S}^2(k) + 2e^{-k^2 \Sigma_{sd}^2/2} [\mathcal{S}(k) \bar{\mathcal{S}}(k) + (b-1)\mathcal{S}(k)] + e^{-k^2 \Sigma_{dd}^2/2} [\bar{\mathcal{S}}^2(k) + 2(b-1)\bar{\mathcal{S}}(k) + (b-1)^2] \right\} \quad (18)$$

which reduces to Eq. (11) in the limit $b \rightarrow 1$. Note that $P_r^{(0)}(k) \rightarrow b^2 P_L(k)$ as $k \rightarrow 0$, as expected, and $P_r^{(0)}(k) \rightarrow$

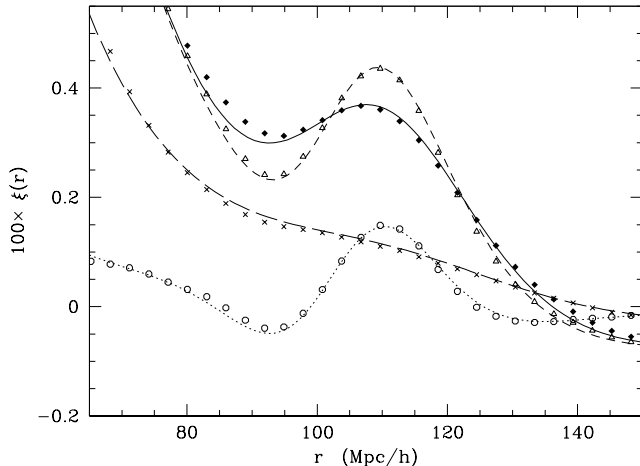


FIG. 7: The correlation functions for the evolved, displaced, shifted and reconstructed fields for halos above $10^{13} h^{-1} M_{\odot}$. Diamonds and the solid line show the final field, crosses and the long-dashed line the shifted field, circles and the dotted line the displaced field and the triangles and short-dashed line the reconstructed field.

$b^2 P_L(k) \exp[-k^2 \Sigma^2/2]$ in the limit that $\Sigma_{ss} = \Sigma_{dd} = \Sigma_{sd}$.

Fig. 7 shows how well this expression, plus the 2nd order contributions, matches the simulations. As with Fig. 4, the agreement is overall quite good, slightly better than for the mass in the case of ξ_f and ξ_r . As in that case, a slight increase in the Σ can improve the agreement somewhat, but we have left the theoretical predictions unchanged.

Just as with the matter field, the smearing of the acoustic peak is reduced by reconstruction. In fact there is relatively little difference between the biased and unbiased tracers in this respect.

IV. CHANGE IN THE PEAK LOCATION

The above sections demonstrate that the LPT provides a good description of how reconstruction reduces the smoothing of the acoustic feature, both for the dark matter and halos. Recent simulations [7] have also found that reconstruction corrects the $\sim 0.5\%$ change in the acoustic scale caused by nonlinear evolution. It is therefore interesting to see how this is manifest within Lagrangian perturbation theory.

In perturbation theory the change in the acoustic peak location comes about because there are second-order corrections to $P(k)$ which are out-of-phase with the linear theory oscillations [6, 7, 8, 9, 14]. The out-of-phase component is quite similar to the derivative of P_L so, by Taylor's theorem, this addition is akin to a change in the characteristic frequency of the oscillation. We consider the analogous terms for the reconstructed power spectrum below, in order to explain how reconstruction suppresses such changes.

These out-of-phase components come about because of the structure of the mode-coupling terms (the Q_n in the notation of Appendix A and Ref. [24]), and this structure is modified

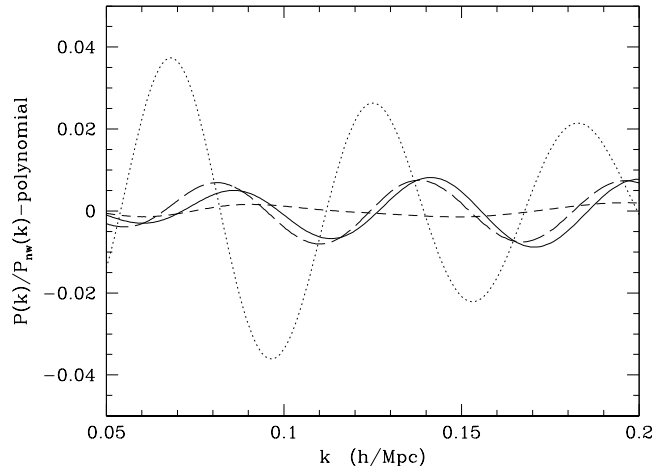


FIG. 8: The out-of-phase pieces of the power spectrum of halos more massive than $10^{13} h^{-1} M_{\odot}$ as predicted by perturbation theory. To emphasize the oscillations, each spectrum has been divided by the “no wiggle” form of Ref. [5] and has had a 4th order polynomial (in k) subtracted. The dotted line shows the linear theory (divided by 2). The solid line is the out-of-phase or mode-coupling pieces of P_f , which can be compared to $dP_L/d \ln k$ (long-dashed line) [10]. The short-dashed line shows that reconstruction reduces the amplitude of the out-of-phase terms and hence the change in the location of the acoustic peak in $\xi(r)$.

by reconstruction in such a way as to reduce the amplitude of the out-of-phase contribution [14]. Figure 8 shows the out-of-phase terms, with the broad-band shape removed to focus on the oscillatory structure, compared to the in-phase acoustic signature in the linear theory. Note that the modification of the mode-coupling terms detailed in the Appendix drastically reduces the amplitude of the out-of-phase terms in the reconstructed spectrum, and hence the change in the acoustic scale. This explains why the change in the peak location seen in simulations is reduced by reconstruction.

V. DISCUSSION

Acoustic oscillations in the photon-baryon fluid prior to decoupling leave an imprint both in the cosmic microwave background anisotropy power spectrum and the matter power spectrum. A comparison of these features at different redshifts provides one of the most promising routes to constraining the expansion history of the Universe. Unfortunately at low redshift, where the accelerated expansion of the Universe is strongest, non-linearities wash out much of the acoustic information.

Recently the authors of Ref. [11] proposed a method for recovering much of the lost information, or reconstructing the acoustic peak. Unfortunately, the method is inherently non-linear and therefore difficult to understand analytically. A study of this problem in Lagrangian perturbation theory [14], for the mass field, shed some light on how the algorithm re-

sulted in tighter constraints on the acoustic scale, but the quantitative validity of Lagrangian perturbation theory is questionable (see e.g. [16] for a recent survey) and we typically study biased tracers of the mass.

We have validated and extended the analytic insights developed in [14], computing a variety of statistics of both the mass density field and the dark matter halo density field using Lagrangian perturbation theory which we then compare to the same quantities measured in a large suite of N-body simulations.

As emphasized in [14], reconstruction does not generate the initial power spectrum or correlation function, but it does serve to sharpen the peak and reduce the change in the peak location associated with non-linearity. We demonstrate explicitly that both of these points remain true for biased tracers. The amount by which the non-linear smearing is reduced is comparable for biased tracers and for the mass, since it is generated by bulk flows which are sourced by the mass density independent of the form of the tracer. The fact that peaks form in special locations in the density field appears to have a very small effect. The reduction in the peak location change due to reconstruction is at least as dramatic for biased tracers as for the mass, with the out-of-phase component responsible for the change being reduced in amplitude by the process of reconstruction. A discussion of by how much the peak position changes depends on a detailed description of the fitting methodology and the sample under consideration, but if we model the observed spectra as in [10] we find that reconstruction reduces the position change by a factor of 2 – 4 for moderately biased tracers like those investigated here.

We conclude that Lagrangian perturbation theory, while not perfect, provides a good framework for thinking about reconstruction. It explains in a natural way how reconstruction works, and how it achieves a reduction in the smearing and position of the acoustic peak generated by non-linear evolution. The predictions of LPT agree to within several percent with the results of N-body simulations on the large scales most relevant to acoustic oscillations, for both biased and unbiased tracers. While not shown explicitly in figures here, perturbation theory becomes an increasingly good description of the simulations at higher redshift, though the need for reconstruction beyond $z \simeq 1$ is greatly reduced.

Acknowledgments

We would like to thank Hee-Jong Seo for useful comments on an early draft of this paper. The simulations presented in this paper were carried out using computing resources of the National Energy Research Scientific Computing Center and the Laboratory Research Computing project at Lawrence Berkeley National Laboratory. MW is supported by NASA and the DoE. This research was additionally supported by the Laboratory Directed Research and Development program at Lawrence Berkeley National Laboratory, and by the Director, Office of Science, of the U.S. Department of Energy under Contract No. DE-AC02-05CH11231.

APPENDIX A: BEYOND LEADING ORDER

Lagrangian perturbation theory allows us to compute corrections to the lowest order expressions for $P(k)$ and $G(k)$ listed in the text. Here we give the 2nd order contributions, following [9, 24] and [10]. The notation and procedure is borrowed heavily from these works, to which we refer the reader for more details.

Recall that the displacement is expanded in powers of the linear density contrast, δ_L , as [27]

$$\begin{aligned} \Psi^{(n)}(\mathbf{k}) &= \frac{i}{n!} \int \prod_{i=1}^n \left[\frac{d^3 k_i}{(2\pi)^3} \right] \\ &\times (2\pi)^3 \delta^{(D)} \left(\sum_i \mathbf{k}_i - \mathbf{k} \right) \\ &\times \mathbf{L}^{(n)}(\mathbf{k}_1, \dots, \mathbf{k}_n, \mathbf{k}) \delta_L(\mathbf{k}_1) \dots \delta_L(\mathbf{k}_n) \end{aligned} \quad (\text{A1})$$

where the $\mathbf{L}^{(n)}$ have closed form expressions, generated by recurrence relations. For example,

$$\mathbf{L}^{(1)} = \frac{\mathbf{k}}{k^2} \quad (\text{A2})$$

is the well known Zel'dovich displacement, which is 1st order LPT.

The density field for a biased tracer can be defined by the displacement field $\Psi(\mathbf{q})$ and a function of the smoothed initial density field in Lagrangian space, $F[\delta_L(\mathbf{q})]$, as

$$\delta_{\text{obj}}(\mathbf{x}) = \int d^3 q F[\delta_L(\mathbf{q})] \delta_D^{(3)}(\mathbf{x} - \mathbf{q} - \Psi), \quad (\text{A3})$$

where \mathbf{x} and \mathbf{q} are the Eulerian and Lagrangian positions and $\delta_D^{(3)}$ is the 3D Dirac δ function. The power spectrum for such tracers can then be written as [9, 24]

$$\begin{aligned} P(k) &= \int d^3 q e^{-i\mathbf{k}\mathbf{q}} \left[\int_{-\infty}^{\infty} \frac{d\lambda_1}{2\pi} \frac{d\lambda_2}{2\pi} \tilde{F}(\lambda_1) \tilde{F}(\lambda_2) \times \right. \\ &\left. \left\langle e^{i(\lambda_1 \delta_L(\mathbf{q}_1) + \lambda_2 \delta_L(\mathbf{q}_2) + i\mathbf{k}[\Psi(\mathbf{q}_1) - \Psi(\mathbf{q}_2)])} \right\rangle - 1 \right], \end{aligned} \quad (\text{A4})$$

where $\mathbf{q} = \mathbf{q}_1 - \mathbf{q}_2$ and \tilde{F} is the Fourier transform of F . The distribution-averaged derivatives of $F(\lambda)$, $\langle F' \rangle$ and $\langle F'' \rangle$, characterize the bias of the sample under consideration. Expressions for the case of peaks in the initial density field (i.e. peaks bias) can be found in [24]. For the halos considered in the text ($M \geq 10^{13} h^{-1} M_\odot$) we have $\langle F' \rangle = 0.55$ and $\langle F'' \rangle = -0.37$, with large-scale bias 1.55.

To obtain the propagator we cross-correlate Eq. (A3) with a field defined by $\exp(i\lambda\delta_L)$; δ_L^n is then simply obtained by taking the n -th derivative with respect to λ and setting λ to zero [10]. This allows us to follow a procedure similar to that in Eq. (A4).

The algebra now follows through as in [9, 24] using the cumulant expansion theorem, and collecting all zero-lag correlators to yield, e.g.

$$\begin{aligned} \langle \delta_L \delta_{\text{obj}} \rangle &\propto \int d^3 q e^{-i\mathbf{k}\mathbf{q}} \\ &\times \left[B_{01}^{10} + \frac{i}{2} B_{02}^{10} + \langle F' \rangle (B_{01}^{11} - i\xi) \right] \end{aligned} \quad (\text{A5})$$

where we have omitted the exponential damping terms for brevity and defined [24]

$$B_{m_1 m_2}^{n_1 n_2} \equiv (-1)^{m_1} \times \langle [\delta_L(\mathbf{q}_1)]^{n_1} [\delta_L(\mathbf{q}_1)]^{n_2} [\mathbf{k}\Psi(\mathbf{q}_1)]^{m_1} [\mathbf{k}\Psi(\mathbf{q}_2)]^{m_2} \rangle_c, \quad (\text{A6})$$

with $\langle \dots \rangle_c$ denoting the connected moments.

Straightforward algebra then yields

$$\langle \delta_L \delta_{\text{obj}} \rangle \propto P_L + \frac{5}{21} R_1 + \frac{3}{7} R_2 + \langle F' \rangle \left(P_L + \frac{3}{7} \{R_1 + R_2\} \right) \quad (\text{A7})$$

where [24]

$$R_n(k) \equiv \frac{k^3}{(2\pi)^2} P_L \int_0^\infty dr P_L(kr) \tilde{R}_n(r) \quad (\text{A8})$$

and

$$\tilde{R}_1 = \int_{-1}^1 d\mu \frac{r^2(1-\mu^2)^2}{1+r^2-2r\mu} \quad (\text{A9})$$

$$\tilde{R}_2 = \int_{-1}^1 d\mu \frac{(1-\mu^2)r\mu(1-r\mu)}{1+r^2-2r\mu} \quad (\text{A10})$$

while for the power spectrum, omitting the damping terms, [24]

$$\begin{aligned} P_{\text{obj}} \propto & (1 + \langle F' \rangle)^2 P_L + \frac{9}{98} Q_1 + \frac{3}{7} Q_2 + \frac{1}{2} Q_3 \\ & + \langle F' \rangle \left[\frac{6}{7} Q_5 + 2Q_7 \right] + \langle F'' \rangle \left[\frac{3}{7} Q_8 + Q_9 \right] \\ & + \langle F' \rangle^2 [Q_9 + Q_{11}] + 2\langle F' \rangle \langle F'' \rangle Q_{12} \\ & + \frac{1}{2} \langle F'' \rangle^2 Q_{13} + \frac{6}{7} (1 + \langle F' \rangle)^2 [R_1 + R_2] \\ & - \frac{8}{21} (1 + \langle F' \rangle) R_1 \end{aligned} \quad (\text{A11})$$

with

$$Q_n(k) \equiv \frac{k^3}{(2\pi)^2} \int_0^\infty dr P_L(kr) \int_{-1}^{+1} d\mu P_L \left[k\sqrt{1+r^2-2r\mu} \right] \tilde{Q}_n(r, \mu) \quad (\text{A12})$$

and expressions for the \tilde{Q}_n can be found in [24].

Extending these results to reconstruction is now relatively straightforward, assuming that the smoothed density field can be well approximated by the linear field. The shifted field has $\Psi = \Psi^{(1)}\mathcal{S}$ and no higher order contributions, while the displaced field can be obtained from Ψ with the replacement $\Psi^{(1)} \rightarrow \Psi^{(1)}[1 - \mathcal{S}]$ with $\Psi^{(n \geq 2)}$ unchanged. This yields

$$\langle \delta_L \delta_s \rangle \propto -P_L \mathcal{S} \quad (\text{A13})$$

$$\begin{aligned} \langle \delta_L \delta_d \rangle \propto & P_L \bar{\mathcal{S}} + \frac{5}{21} R_1 + \frac{3}{7} R_2^{(d)} \\ & + \langle F' \rangle \left(P_L + \frac{3}{7} \{R_1 + R_2\} \right) \end{aligned} \quad (\text{A14})$$

where $\bar{\mathcal{S}} \equiv (1 - \mathcal{S})$ and $R_2^{(d)}$ is evaluated using $P_L \bar{\mathcal{S}}$ inside the integral Eq. (A8).

The power spectrum can be evaluated in a similar fashion, with the three contributions being

$$P^{ss} \propto P_L \mathcal{S}^2 + \frac{1}{2} Q_3^{(ssss)} \quad (\text{A15})$$

and

$$\begin{aligned} P^{sd} + P^{ds} \propto & -2P_L \mathcal{S} \bar{\mathcal{S}} + \frac{3}{7} Q_2^{(1s1s)} + Q_3^{(sdsd)} \\ & - \mathcal{S} \left[\frac{10}{21} R_1 + \frac{6}{7} R_2^{(d)} \right] \\ & + \langle F' \rangle \left[-2SP_L + 2Q_7^{(1sds)} \right. \\ & \left. - \frac{6}{7} \mathcal{S} (R_1 + R_2) \right] \\ & + \langle F'' \rangle Q_9^{(1s1s)} \end{aligned} \quad (\text{A16})$$

and

$$\begin{aligned} P^{dd} \propto & P_L \bar{\mathcal{S}}^2 + \frac{9}{98} Q_1 + \frac{3}{7} Q_2^{(1d1d)} + \frac{1}{2} Q_3^{(dddd)} \\ & + \bar{\mathcal{S}} \left[\frac{10}{21} R_1 + \frac{6}{7} R_2^{(d)} \right] \\ & + \langle F' \rangle \left[2P_L \bar{\mathcal{S}} + \frac{6}{7} Q_5^{(1d11)} + 2Q_7^{(1ddd)} + \right. \\ & \left. \frac{10}{21} R_1 + \frac{6}{7} R_2^{(d)} + \frac{6}{7} \bar{\mathcal{S}} (R_1 + R_2) \right] \\ & + \langle F'' \rangle \left[\frac{3}{7} Q_8 + Q_9^{(1d1d)} \right] \\ & + \langle F' \rangle^2 \left[P_L + \frac{6}{7} (R_1 + R_2) + Q_9^{(1d1d)} + Q_{11}^{(11dd)} \right] \\ & + 2\langle F' \rangle \langle F'' \rangle Q_{12}^{(111d)} + \frac{1}{2} \langle F'' \rangle^2 Q_{13} \end{aligned} \quad (\text{A17})$$

where we have again omitted the damping terms and the superscripts indicate which P_L are to be replaced with $P_L \mathcal{S}$, $P_L \bar{\mathcal{S}}$ etc. For the Q_n there are 4 possible smoothing terms, and we have indicated no smoothing with a 1, \mathcal{S} with an s and $\bar{\mathcal{S}}$ with a d . The first two terms have argument kr and the second have argument $k\sqrt{1+r^2-2r\mu}$ in Eq. (A12). Thus for example

$$\begin{aligned} Q_7^{(1sds)}(k) = & \frac{k^3}{(2\pi)^2} \int_0^\infty dr P_L(kr) \mathcal{S}(kr) \\ & \times \int_{-1}^{+1} d\mu P_L(ky) \mathcal{S}(ky) \bar{\mathcal{S}}(ky) \\ & \times \tilde{Q}_7(r, \mu) \end{aligned} \quad (\text{A18})$$

with $y = \sqrt{1+r^2-2r\mu}$.

-
- [1] P. J. E. Peebles and J. T. Yu, *Astrophys. J.* **162**, 815 (1970).
 - [2] R. A. Sunyaev and Y. B. Zeldovich, *Astrophys. Space Science* **7**, 3 (1970).
 - [3] A. G. Doroshkevich, Y. B. Zel'Dovich, and R. A. Sunyaev, *Soviet Astronomy* **22**, 523 (1978).
 - [4] A. Meiksin, M. White, and J. A. Peacock, *Mon. Not. R. Astron. Soc.* **304**, 851 (1999), arXiv:astro-ph/9812214.
 - [5] D. J. Eisenstein and W. Hu, *Astrophys. J.* **496**, 605 (1998), arXiv:astro-ph/9709112.
 - [6] D. J. Eisenstein, H.-J. Seo, and M. White, *Astrophys. J.* **664**, 660 (2007), arXiv:astro-ph/0604361.
 - [7] H.-J. Seo, E. R. Siegel, D. J. Eisenstein, and M. White, *Astrophys. J.* **686**, 13 (2008), 0805.0117.
 - [8] M. Crocce and R. Scoccimarro, *Phys. Rev. D* **77**, 023533 (2008), 0704.2783.
 - [9] T. Matsubara, *Phys. Rev. D* **77**, 063530 (2008), 0711.2521.
 - [10] N. Padmanabhan and M. White, *ArXiv e-prints* (2009), 0906.1198.
 - [11] D. J. Eisenstein, H.-J. Seo, E. Sirko, and D. N. Spergel, *Astrophys. J.* **664**, 675 (2007), arXiv:astro-ph/0604362.
 - [12] E. Huff, A. E. Schulz, M. White, D. J. Schlegel, and M. S. Warren, *Astroparticle Physics* **26**, 351 (2007), arXiv:astro-ph/0607061.
 - [13] C. Wagner, V. Müller, and M. Steinmetz, *Astron. Astrophys.* **487**, 63 (2008), 0705.0354.
 - [14] N. Padmanabhan, M. White, and J. D. Cohn, *Phys. Rev. D* **79**, 063523 (2009), 0812.2905.
 - [15] M. White, *Astrophys. J. Supp.* **143**, 241 (2002), arXiv:astro-ph/0207185.
 - [16] J. Carlson, M. White, and N. Padmanabhan, *ArXiv e-prints* (2009), 0905.0479.
 - [17] M. Davis, G. Efstathiou, C. S. Frenk, and S. D. M. White, *Astrophys. J.* **292**, 371 (1985).
 - [18] R. W. Hockney and J. W. Eastwood, *Computer simulation using particles* (Bristol: Hilger, 1988, 1988).
 - [19] T. Buchert, *Astron. Astrophys.* **223**, 9 (1989).
 - [20] F. Moutarde, J.-M. Alimi, F. R. Bouchet, R. Pellat, and A. Ramani, *Astrophys. J.* **382**, 377 (1991).
 - [21] E. Hivon, F. R. Bouchet, S. Colombi, and R. Juszkiewicz, *Astron. Astrophys.* **298**, 643 (1995), arXiv:astro-ph/9407049.
 - [22] A. N. Taylor and A. J. S. Hamilton, *Mon. Not. R. Astron. Soc.* **282**, 767 (1996), arXiv:astro-ph/9604020.
 - [23] S. Bharadwaj, *Astrophys. J.* **472**, 1 (1996), arXiv:astro-ph/9606121.
 - [24] T. Matsubara, *Phys. Rev. D* **78**, 083519 (2008).
 - [25] J. M. Bardeen, J. R. Bond, N. Kaiser, and A. S. Szalay, *Astrophys. J.* **304**, 15 (1986).
 - [26] W. J. Percival and B. M. Schäfer, *Mon. Not. R. Astron. Soc.* **385**, L78 (2008), 0712.2729.
 - [27] F. R. Bouchet, S. Colombi, E. Hivon, and R. Juszkiewicz, *Astron. Astrophys.* **296**, 575 (1995), arXiv:astro-ph/9406013.